inorganics

MDPI

Article

Pyridine vs. Thiazole in Cyclometalated NˆCˆN Ni(II) Complexes

Lukas Kletsch [1], Rose Jordan [1], Julian Strippel [1], David A. Vicic [2] and Axel Klein [1,*]

[1] University of Cologne, Faculty of Mathematics and Natural Sciences, Department of Chemistry and Biochemistry, Institute for Inorganic and Materials Chemistry, Greinstraße 6, D-50939 Koeln, Germany; lukas.kletsch@uni-koeln.de (L.K.); rose.jordan@uni-koeln.de (R.J.); jstrippe@smail.uni-koeln.de (J.S.)

[2] Lehigh University, Department of Chemistry, 6 East Packer Ave, Bethlehem, PA 18015, USA; dav512@lehigh.edu

* Correspondence: axel.klein@uni-koeln.de; Tel.: +49-221-470-4006

Abstract: Six NˆCˆN cyclometalated Ni(II) complexes [Ni(NˆCˆN)Cl] or [Ni(NˆCˆN′)Br] with symmetric NˆCˆN or non-symmetric NˆCˆN′ ligands in which the peripheral N-groups were varied with pyridine (Py), 4-thiazole (4Tz), 2-thiazole (2Tz), and 2-benzothiazole (2Btz) complementing the previously reported complexes with di(2-pyridyl)phenide ligands [Ni(Py(Ph)Py)X] X = Cl or Br. The non-symmetric [Ni(NˆCˆN′)Br] complexes were synthesized from $NiBr_2$ and NˆCHˆN′ protoligands through base-assisted nickelation, while the symmetric [Ni(NˆCˆN)Cl] complexes were received from the NˆC(Cl)ˆN protoligands and $[Ni(COD)_2]$ (COD = 1,5-cyclooctadiene). Introduction of 4Tz on both sides shifted the electrochemical gap $\Delta E_{exp} = E_{ox}–E_{red}$ and the long wavelength UV-vis absorption maxima of the complexes to higher energies, while 2Tz leads to a shift to lower energies. When introducing only one 4Tz or 2Tz as peripheral groups, the remaining PhPy moiety dominates the electronic properties and electrochemistry and photophysics are very similar to the Py(Ph)Py derivatives. In contrast to this, introduction of 2Btz shifts both values to lower energies, regardless of one or two 2Btz groups and the 2Btz moiety dominates the character of the frontier molecular orbitals of the complexes, as DFT calculations show. Long-wavelength UV-vis absorptions vary from 416 to 443 nm, and their energies correlate well with the first reduction potentials. Negishi-type C–C cross-coupling reactions gave total yields ranging from 1 to 60% and cross-coupling yields from 1 to 44%. The reactivities correlate roughly with the first reduction potentials. Facilitated reduction (*E* around –2 or higher) goes generally along with improved performance, making the thiazole-containing complexes interesting candidates for such catalysis.

Keywords: nickel; NCN cyclometalated; thiazole; electronic structure; Negishi-type cross-coupling

check for updates

Academic Editor: Alex Chun-Yuen Wong

Received: 2 December 2024
Revised: 27 January 2025
Accepted: 27 January 2025
Published: 1 February 2025

Citation: Kletsch, L.; Jordan, R.; Strippel, J.; Vicic, D.A.; Klein, A. Pyridine vs. Thiazole in Cyclometalated NˆCˆN Ni(II) Complexes. *Inorganics* **2025**, *13*, 41. https://doi.org/10.3390/inorganics13020041

Copyright: © 2025 by the authors. Licensee MDPI, Basel, Switzerland. This article is an open access article distributed under the terms and conditions of the Creative Commons Attribution (CC BY) license (https://creativecommons.org/licenses/by/4.0/).

1. Introduction

Due to their exceptional activity in C–C coupling catalysis, Pd complexes are nowadays quintessential in the field of organic synthesis [1]. A serious drawback of Pd-based cross-coupling catalysis, for which Heck, Negishi, and Suzuki received the 2010 Nobel Prize in chemistry [1], is the high cost and limited availability of the noble metal Pd [2]. This motivates research into cheaper and more abundant alternatives, which from a sustainability and cost–benefit perspective may be preferable even at significantly lower efficiency. An obvious candidate for the replacement of Pd is its lighter homologue Ni, the catalytic activity in C–C cross-coupling reactions of which has been discovered even before that of Pd in the early 1900s [2]. Significant advances in this area have been reported in recent years [3–12]. As the scope and mechanism of Ni-catalyzed C–C cross-coupling reactions is very diverse,

current research is focused on mechanistic studies and the development of new catalytically active Ni complexes for the synthesis of organic compounds, some of which are not even accessible through Pd-mediated reactions [2–4]. One somewhat underrepresented class of compounds among Ni-based cross-coupling catalysts are cyclonickelated pincer ligand complexes, probably due to their comparatively low stability, which might however also be a positive feature if catalysis could be controlled [10–13]. We have contributed to this using Ni(II) complexes [Ni(CˆNˆN)X] (X = F,Cl, Br, I) with cyclometalating CˆNˆN ligands of the 6-phenyl-2,2′-bipyridine type for Negishi-type C–C cross-coupling [14], trying to replace the established [Ni(terpy)X] (X = Cl, Br, I, Me) complexes [15–18].

When moving on to organonickel(II) complexes [Ni(NˆCˆN)X] containing NˆCˆN-type cyclometalated ligands, we can state a surge in relevance in the scientific literature only in very recent years [13,19–21], which is due to their much more difficult synthesis compared with the established Pt(II) and Pd(II) derivatives (Scheme 1).

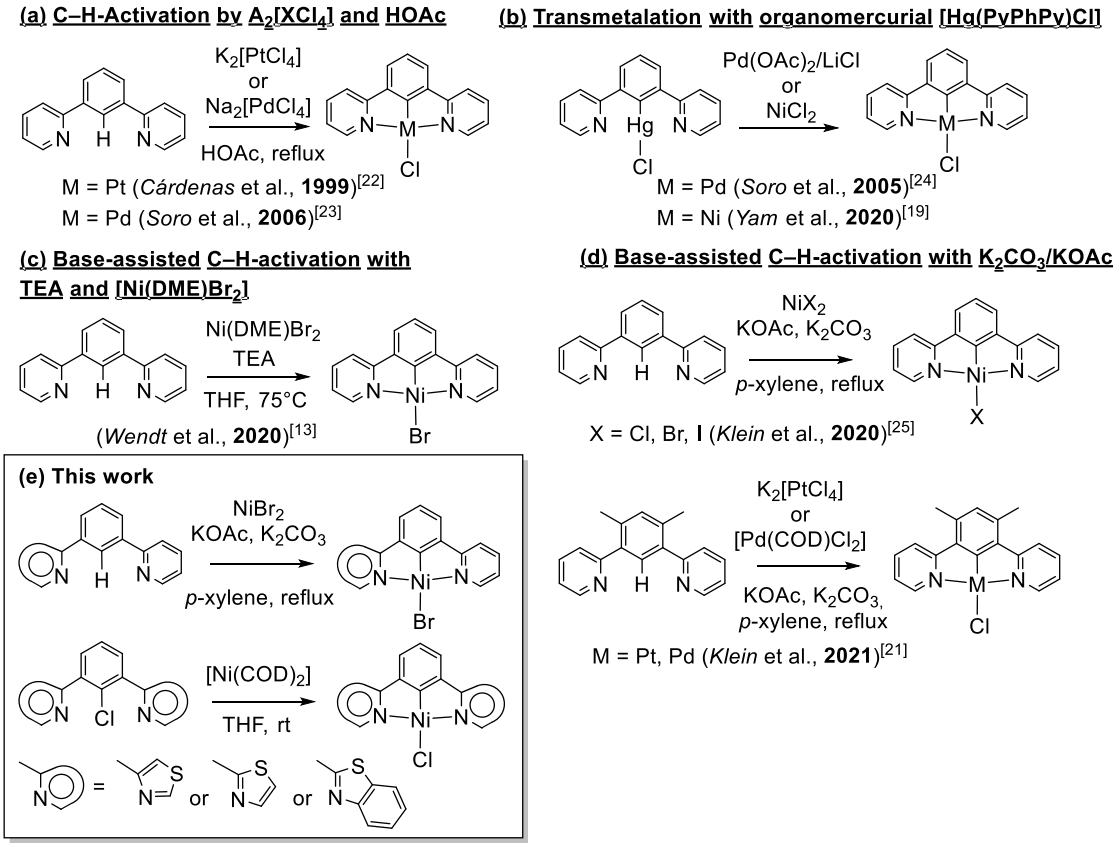

Scheme 1. Strategies for the synthesis of cyclometalated Ni(II), Pd(II), and Pt(II) complexes bearing dipyridylbenzene (dpb) ligands: (**a**) C–H activation by $A_2[MCl_4]$ (M = Pt, Pd) and HOAc [22,23]; (**b**) transmetalation with organomercurial [Hg(Py(Ph)Py)Cl] [19,24]; (**c**) base-assisted C–H activation with TEA and $[Ni(DME)Br_2]$ [13]; (**d**) base-assisted C–H activation with K_2CO_3/KOAc [25]; (**e**) this work: introduction of thiazole or benzothiazole-containing complexes through oxidative addition for symmetric NˆCˆN systems and through base-assisted C–H activation for non-symmetric NˆCˆN′ ligands [21].

While their Pt(II) and Pd(II) congeners are readily accessible via facile C–H activation in HOAc (Scheme 1a) [22,23], e.g., [Ni(Py(Ph)Py)X] (Py(Ph)Py = 2,6-di(2-pyridyl)phenide) derivatives require more involved methods for their synthesis. In 2020, three different groups independently reported synthesis conditions for [Ni(Py(Ph)Py)X] (X = Cl or Br), including transmetalation from an organomercury intermediate [24] reported by Yam et al. (Scheme 1b) [19], as well as two different base-assisted methods reported by Wendt et al.

(Scheme 1c) and our group (Scheme 1d) [13,20]. The base-assisted route using a combination of K_2CO_3 and KOAc, originally developed at our group for CˆNˆN-type complexes [Ni(CˆNˆN)X] [25], was also recently applied to Pd and Pt (Scheme 1d) [21]. Alternatively, CˆNˆN Ni(II) complexes were prepared through C–X activation (oxidative addition) from halogenated protoligands and $[Ni(COD)_2]$ (COD = 1,5-cyclooctadiene) [26–28].

A natural next step from [Ni(Py(Ph)Py)X] is the variation of the pincer ligand backbone in order to tune the properties of the complexes. For corresponding [Pt(NˆCˆN)Cl] complexes, the replacement of the peripheral pyridines to quinolines and pyrimidine have been reported [29–31]. They have been introduced to alter the electrochemical and photophysical properties. In general, the introduction of quinolines or pyrimidines led to facilitated electrochemical reduction and to red-shifted absorptions and emissions compared with the parent Py(Ph)Py systems. A study replacing pyridine on one or both sites by 1-pyrazolyl units showed lower reduction potentials (more negative) and blue-shifted absorptions and emissions [32]. The electronic changes upon exchange of pyridine to 1-pyrazole were later investigated in a quantum chemical study and confirmed the experimental work [33]. The complex [Pt(Py(Ph)Pz)Cl] (Pz = 1*H*-pyrazol-3-yl) was used as building block for diphosphine-bridged dinuclear complexes [34]. Replacing one pyridine by 3-(2-oxazoline) groups allowed to observe circularly polarized luminescence from helical aggregates and overall red-shifted absorptions and emission in solution [35]. The introduction of purine gave an NˆC*N′ structural motive with a six-ring phenyl-purine C*N′ chelate moiety in addition to a five-ring phenyl-pyridine NˆC chelate [36]. This led to blue-shifted absorption and emission and enhanced tendency to form aggregates through π···π stacking and Pt···Pt interactions. From Pd(II), only complex [Pd(NˆCˆN′)Cl] with N′ = 2-oxazolinyl has been reported [37]. The authors used the above-mentioned mercuration method for the synthesis and reported catalytic activity in Suzuki coupling and a blue-shifted absorption [37] compared to the Pt(II) 2-oxazoline derivative mentioned above [35].

In contrast to this, thiazoles or benzothiazoles in place of the pyridine moieties have not been reported, but filed in a few patents for Pt only [38,39]. This is remarkable as for CˆNˆN-type complexes with Pd and Pt, (benzo)thiazoles have previously been used as peripheral N moieties [40–44]. While especially for the replacement of pyridine units with thiazole, little change in optical properties was observed, more variation occurred in the oxidation potentials of analogous complexes containing pyridine *versus* five-membered aryl moieties [40–42]. The latter is highly relevant for cross-coupling catalysis. However, no catalysis was reported in all these publications.

Herein we report the synthesis of derivatives of the [Ni(Py(Ph)Py)X] system, using thiazoles and benzothiazoles as the five-membered aryl moieties replacing pyridine in the Py(Ph)Py ligand *6–6–6 ring* scaffold. We chose to study both symmetric (palindromic) ligands *5–6–5 ring* and non-symmetric (non-palindromic) ligands *5–6–6 ring* in order to probe the extent of functional similarity between pyridine and (benzo)thiazole. Furthermore, we are interested in studying the effect of decreased symmetry on the properties of these Ni NˆCˆN complexes using electrochemical methods and UV-vis absorption spectroscopy. The idea of focusing on the symmetry was fueled by recent work by Feuerstein and Breher regarding the group theoretical differences and photophysical properties of di(phenidyl)pyridine (CˆNˆC) Pd(II) complexes compared to their non-palindromic CˆCˆN isomers [45]. In particular, the electrochemical reduction potentials are the rationales along which we will correlate the structure of these complexes with their performance in Negishi-type C–C cross-coupling.

2. Results and Discussion

2.1. Preparation and Analytical Characterization

The synthesis of the symmetric NˆCHˆN and NˆC(Cl)ˆN and non-symmetric NˆCHˆN′ protoligands is described together with their characterization through ^{1}H and ^{13}C nuclear magnetic resonance (NMR) spectra, elemental analyses, and electron ionization mass spectrometry in the positive mode (EI(+)-MS) in the Supplementary Materials.

The synthesis of the Ni(II) complexes was first attempted starting from the NˆCHˆN and NˆCHˆN′ protoligands and $NiBr_2$ using the base-assisted method (Scheme 2a,b) [20,21]. Previously, we were able to synthesize [Ni(Py(Ph)Py)Br] containing the parent *6–6–6 ring* ligand system (Scheme 2a) [20,21]. Within this work, the same method allowed the synthesis of Ni(II) complexes [Ni(4Tz(Ph)Py)Br] (**4**), [Ni(2Tz(Ph)Py)Br] (**5**), and [Ni(2Btz(Ph)Py)Br] (**6**) containing the non-symmetric *5–6–6 ring* ligand systems (Scheme 2b; naming and numbering, see Scheme 3) with yields of 77 (**4**), 64 (**5**), and 47% (**6**). The same reaction failed for the symmetric *5–6–5 ring* NˆCˆN ligand systems (Scheme 2c). Instead the oxidative addition reaction using the chlorido-substituted ligand NˆC(Cl)ˆN and Ni(0) was successful (Scheme 2d) and allowed to synthesize [Ni(4Tz(Ph)4Tz)Cl] (**1**), [Ni(2Tz(Ph)2Tz)Cl] (**2**), and [Ni(2Btz(Ph)2Btz)Br] (**3**) with a yield of 82% for **2** and quantitative yields for **1** and **3** (for details and analytics, see Materials and Methods, Section 3).

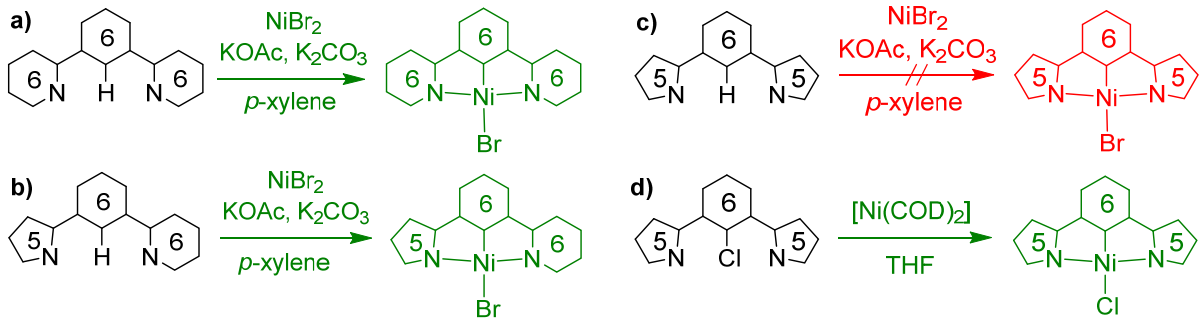

Scheme 2. (**a**) *6–6–6 ring* and (**b**) *5–6–6 ring* NˆCHˆN ligand systems were transformed into Ni(II) complexes via C–H activation. (**c**) *5–6–5 ring* NCN ligand systems failed to produce the Ni(II) complex via C–H activation. (**d**) Oxidative addition reaction using chlorido-substituted ligand NˆC(Cl)ˆN and Ni(0) was successful.

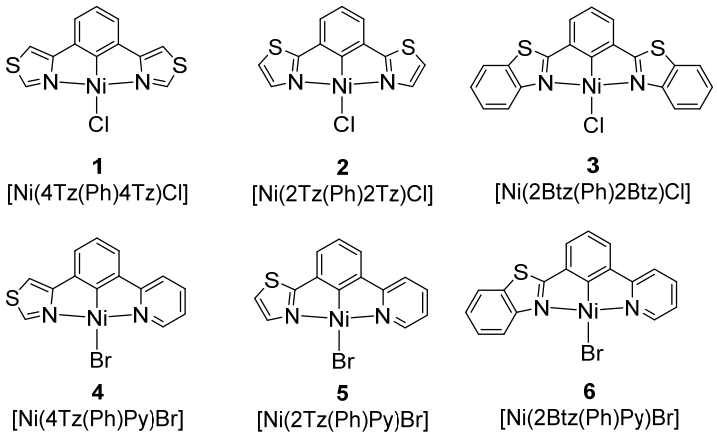

Scheme 3. Ni(II) complexes of this study with abbreviations and numbering.

Thus, we were able to produce six new complexes (Scheme 3) and analyzed them unequivocally through elemental analysis and ^{1}H NMR spectroscopy (spectra and data in the Supplementary Materials, SM).

The failure to synthesize the symmetric complexes containing the *5–6–5 ring* NˆCˆN ligands through C–H activation is either caused by the slightly lower basicity of (benzo)thiazoles compared with pyridine (pK_A of HTz^+ = 2.44, HPy^+ = 5.23) [46], or is due to the larger NˆC bite angles for the peripheral *5 ring*- compared with the *6 ring*-aryl moieties. Assuming a pre-coordination of the Ni(II) to the peripheral N atom proceeding the cyclometalation, a weaker Ni–N pre-coordination for the weaker base thiazole might slow down the pre-coordination, thus hampering the overall complex formation. Alternatively the NˆC–H bite angle probably larger for the peripheral *5 rings*, which is hampering the cyclometalation, as the distance between the pre-coordinated Ni(II) and the H–C function is enlarged compared with the *6-ring* system.

2.2. X-Ray Diffractometric Analysis of Single Crystals (scXRD) and DFT-Calculated Structures

The crystal and molecular structure of all six compounds were studied through scXRD, **6** crystalized as THF solvate (**6**.0.5THF) (Figures S74–S80 in the Supplementary Materials (SM) show the structures). Tables with the structure solution and refinement, as well as tables listing essential bond metrics of the six complexes are provided in Tables S1–S4 (Supplementary Materials). They show that none of the structures was found to be isostructural to the previously reported complexes [Ni(Py(Ph)Py)X] (X = Cl, Br, I) [20]. For **1**, the same space group was found ($P\,2_1/n$), but we refined an asymmetric unit containing five independent molecular units, one of which is disordered, with 86% occupancy for the molecules oriented in one direction and 14% in the opposite direction. Nevertheless, the new structures share the typical head-to-tail arrangement of two molecules with the parent Py(Ph)Py containing complexes [20]. In all six structures, we found extensive π···π stacking with different stacking motives. While the molecules in the structure of **1** and **3** are stacked pair-wise head-to-tail (Figures S75 and S77, Supplementary Materials), all head-to-tail "dimers" in the structures of **2** and **4** are aligned in parallel sheets (Figures S76 and S79, Supplementary Materials). In complexes **4** and **6**, the head-to-tail dimers are part of columns along the crystallographic *a* axis (Figures S78 and S80, Supplementary Materials).

For **5**, the two peripheral groups were refined with mixed occupancies (pyridine/2-thiazole) (Figure S79, Supplementary Materials). Expansion of the asymmetric unit in a space group of lower symmetry, e.g., *P*-1, did not serve to resolve the disorder and individually localize the two groups, which indicates a true, statistical pyridine/2-thiazole disorder.

The molecular structures show a distorted square-planar coordination of the Ni(II) centers, with the largest distortion from "square" caused by the N–Ni–N angles ranging from 161 to 164°, thus deviating from the ideal 180° in a perfect square (Figure 1). Minor distortions occur for the C–Ni–X bonds with values markedly below 180° for **1** (173°), **3** (165°), **4**, and **6**·0.5THF (both 171°).

Overall, the metrics of the six Ni(II) (benzo)thiazole complexes agree quite well with those of the [Ni(Py(Ph)Py)X] (X = Cl or Br) derivatives (Tables S2 and S4, Supplementary Materials). More importantly, the density functional theory (DFT) calculated metrics agree very well with the experimental structures of the six new complexes (Tables S5 and S6, Supplementary Materials).

Furthermore, the failure to synthesize the symmetric complexes containing the *5–6–5 ring* NˆCˆN ligands through C–H activation cannot simply be explained from the different ring-sizes of the peripheral N moieties Py (*6 ring*) vs. Tz or Btz (*5 ring*). The final products do not show any differences both in terms of bond lengths or angles around Ni, nor in the DFT-calculated energies.

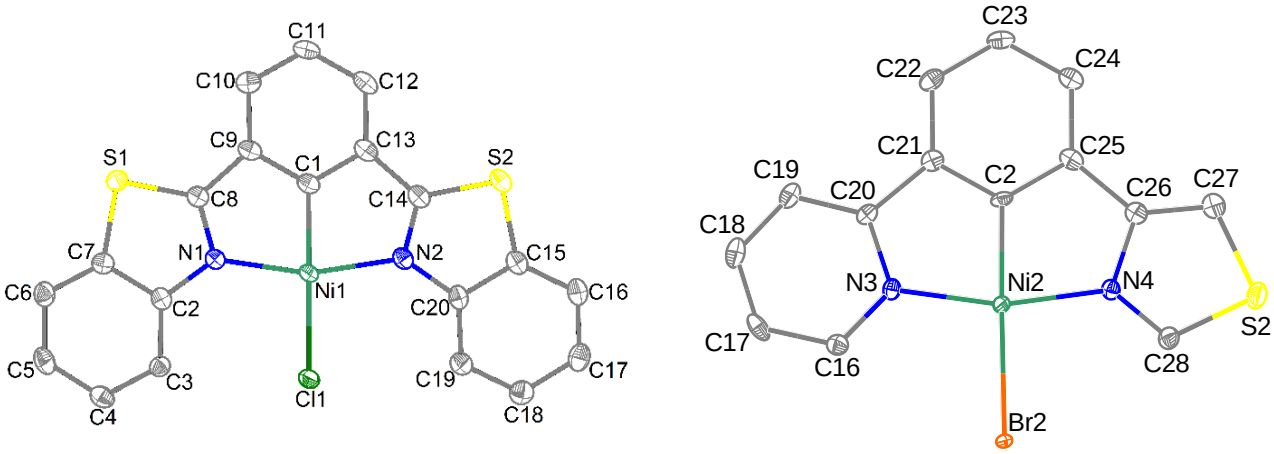

Figure 1. Molecular structures of **3** (left) and **4** (right, shown is one out of two independent molecules) from sc-XRD, thermal ellipsoids at 50% probability, H atoms omitted for clarity.

2.3. Electrochemistry and DFT Calculations of Frontier Orbitals

The complexes show a rich electrochemistry in cyclic voltammograms in THF solution (Figures 2, 3, S81 and S82, Supplementary Materials) with several reductions in the range from −2 to −3.3 V and one or two oxidation waves slightly above 0 V vs. the ferrocene/ferrocenium couple (Figure 3, full data in Table S7, Supplementary Materials). Both the first oxidation and the first reduction are one-electron processes as confirmed through measurements on weighted samples.

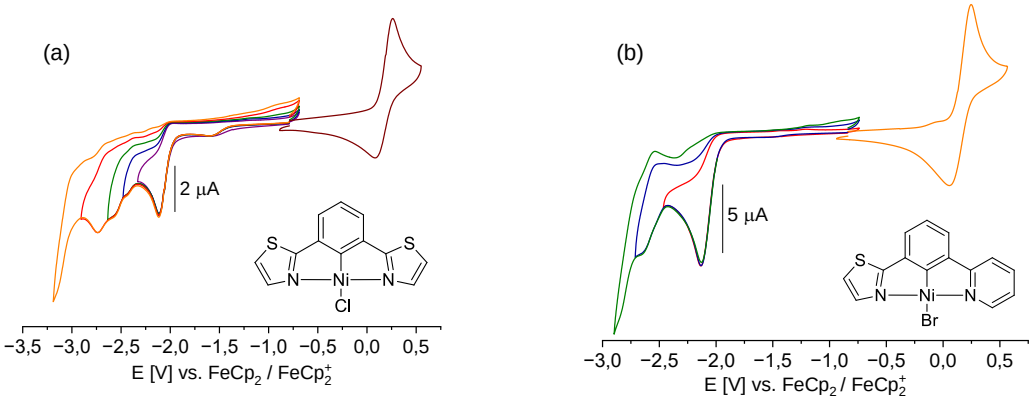

Figure 2. Cyclic voltammograms of (**a**) [Ni(2Tz(Ph)2Tz)Cl] (**2**) and (**b**) [Ni(2Tz(Ph)Py)Br] (**5**) in 0.1 M *n*-Bu_4NPF_6/THF solution at room temperature and 100 mV/s scan rate.

Following the DFT-calculated composition of the lowest unoccupied molecular orbitals (LUMO), the first reductions can be assigned to ligand-centered processes with contributions from the central Ph unit and the peripheral Tz units for symmetric complexes **1** to **3** (Figure 3, more details in Figure S84). For the non-symmetric complexes, the LUMO is essentially localized in the Ph(Py) moiety for **4** [Ni(4Tz(Ph)Py)Br], while for the 2Tz derivative **5** and the 2Btz complex **6**, the LUMO is found delocalized over the 2Tz(Ph) and 2Btz(Ph) units (Figures 3 and S85).

For both series, The LUMO energy is highest for the 4Tz complexes (**1** and **4**), followed by the 2Tz (**2** and **5**) and the 2Btz derivatives (**3** and **6**) in keeping with the increasing electrochemical reduction potentials along the series 4Tz < 2Tz < 2Btz (Table S7). At the same time, the energies are markedly lower for the symmetric variant of the three pairs of complexes. Overall, the DFT-calculated compositions and energies of the first and second LUMO (LUMO+1) are in line with essentially ligand-centered electrochemical reductions,

and the slightly different orbital situation explains the different reduction behavior in terms of number of individual waves (Figures S81 and S82, Supplementary Materials). This is also in agreement with similar Pt(II) and Pd(II) complexes containing CˆNˆN ligands with peripheral thiazole moieties [40–42] and the parent [Ni(Py(Ph)Py)X] complexes [20,21]. The lowest metal-centered antibonding d* orbital, the d_{x2-y2} is found slightly above the LUMO (~0.5 eV) as LUMO+2 for all six complexes. In view of the same observations made for the parent [Ni(Py(Ph)Py)X] (X = Cl or Br) complexes [20,21] and their CˆNˆN derivatives [14,27], the irreversible nature of the first reduction can be explained through an *EC* mechanism [47], including the electrochemical reduction (*E*) of the complexes to yield $[Ni(N^{\wedge}C^{\wedge}N)Cl]^{\bullet-}$ containing a reduced radical $N^{\wedge}C^{\wedge}N^{\bullet-}$ anionic ligand bound to Ni(II), followed by the "chemical" reaction (*C*), which is the cleavage of the Cl^- or Br^- co-ligand. This produced the reduced species [Ni(NˆCˆN)(solv)] (solv = solvent). Such reduced, formally [Ni(I)] or [Ni(II)(reduced ligand)], species are established as the active catalysts for Negishi-type C–C cross-coupling using Ni(II) precatalysts [3,4,9,12,14,16,18,26,48]. To be able to vary the reduction potentials for the complexes **1** to **6** from −1.72 for **3** to −2.42 for **1**, compared with the approximate −2.3 V for the [Ni(Py(Ph)Py)X] (X = Cl or Br) derivatives (Table S7), makes us confident that the structural variation also leads to markedly varied reactivity in the cross-coupling reaction (see later).

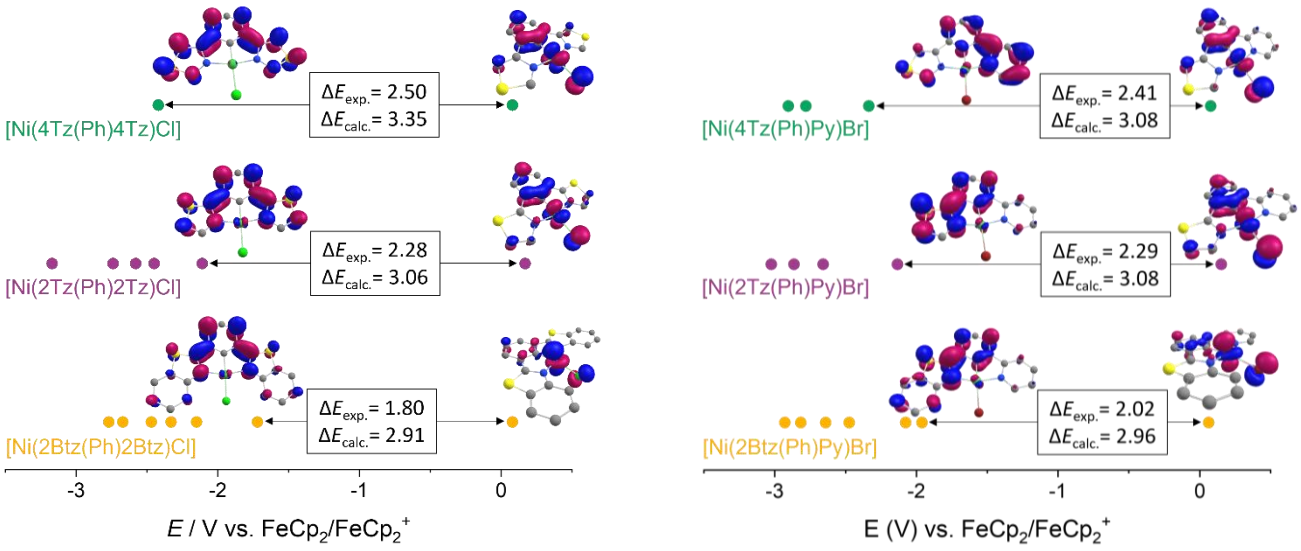

Figure 3. Redox potentials from cyclic voltammetry of symmetric [Ni(NˆCˆN)Cl] (left) and non-symmetric complexes [Ni(NˆCˆN′)Br] (right) described as dots, including electrochemical gap $\Delta E_{exp.}$ (= E_{ox}–E_{red}) and DFT-calculated HOMO-LUMO gaps $\Delta E_{calc.}$ (= E_{HOMO}–E_{LUMO}) and frontier molecular orbital surfaces of HOMO (for oxidation) and LUMO (reduction side).

The highest occupied molecular orbitals (HOMO) are distributed over the central Ph(π)–Ni(d_{xz})–Cl(p_z) moiety for the thiazole complexes **1**, **2**, **4**, and **5** (Figures S2 and S84, Supplementary Materials). The HOMO-1 can be described as having a very large d_{z2} component. For the benzothiazole derivatives **3** and **6**, the HOMO is localized on the Ni(d_{z2})–Cl(p_z) moiety. The HOMO-1 for **3** features essential contributions from the Ph(π)–Ni(d_{z2}) unit, while for **6** an almost pure Ni(d_{z2}) orbital represents the HOMO-1. Thus, the reversible electrochemical oxidations are essentially Ni-centered (Ni(II)/Ni(III) redox pair) as has also been reported for the parent [Ni(Py(Ph)Py)X] complexes [20,21]. While the 4Tz complexes **1** and **3** but also the 2Btz derivatives **4** and **5** show essentially the same oxidation potentials as the parent complexes (~0.07 V), the 2Tz derivatives show higher oxidation potentials by nearly 0.1 eV, which reflects stronger σ-donating power of 2Tz over Py, 4Tz and 2Btz. The calculated HOMO energies agree quite well with this for the comparison 4Tz/2Tz, but the 2Btz values were found to be slightly

below those of 2Tz in both the symmetric and the non-symmetric series. In view of the Negishi-type C–C cross-coupling, the formal Ni(III) oxidation state is important [3,4,9,11,12,14,16,18] in that the lower the oxidation potential of these species, the higher is the stability of the Ni(III) species prior to reductive elimination, producing the R–R' coupling product. However, as the Ni(II)/Ni(III) potentials within our series are largely constant, we do not expect an impact of our structure variation on the C–C cross-coupling efficiency from this mechanistic aspect.

As suggested by Koopmans' and Janak's theorems [49–51], we compared the DFT-calculated HOMO-LUMO gaps ($\Delta E_{\text{HOMO-LUMO(calc)}}$) with the electrochemical gaps ($\Delta E_{\text{redox(exp)}}$). We found that $\Delta E_{\text{HOMO-LUMO(calc)}}$ values range from 2.91 to 3.35 eV and were generally larger than the $\Delta E_{\text{redox(exp)}}$ values ranging from 1.80 to 2.50 eV (Figure 3, $\Delta E_{\text{redox(exp)}}$ in Table 1). Both show the same trends, in that the smallest values are found for the benzothiazole complexes **3** and **6**, while the highest were observed for the 4Tz derivatives **1** and **4**. For the two complexes [Ni(Py(Ph)Py)X], the DFT-calculated ΔEs are very similar (Cl: 3.08; Br: 3.09 eV) as were the experimental values (2.39 and 2.37 eV) [20] and, as for the new thiazole derivatives, the calculated values are markedly higher. The symmetric 4Tz complex **1** shows the highest value, followed by [Ni(Py(Ph)Py)Cl], while the 2Tz (**2**) and especially the 2Btz (**3**) derivatives show far lower values. This is in line with markedly superior electron-accepting properties of 2Tz and 2Btz over 4Tz, while the parent Py group is a slightly better electron-acceptor compared with 4Tz. The value for the non-symmetric (Py-containing) 4Tz complex **4** is very close to that of the parent [Ni(Py(Ph)Py)Br] complex as their redox-chemistry is dominated by the Ph(Py) moiety. The complexes **2**, **3**, and **6**, containing 2Tz or 2Btz units, show markedly smaller values, in line with the Ph(2Tz) or Ph(2Btz) moieties dominating the redox chemistry.

Table 1. Selected electrochemical and photophysical data.

	$\Delta E_{\text{redox(exp.)}}$ (eV) [a]	$\Delta E_{\text{HOMO-LUMO(calc)}}$ (eV) [b]	$\lambda_{\text{max(exp.)}}$ (nm) [c]	$\Delta E_{\text{opt(exp.)}}$ (eV) [d]	$\lambda_{\text{max(calc.)}}$ (nm) [e]	$\Delta E_{\text{opt(calc.)}}$ (eV) [f]
[Ni(Py(Ph)Py)Cl] [g]	2.39	3.08 [c]	437	2.84	469	2.64
[Ni(4Tz(Ph)4Tz)Cl] (**1**)	2.50	3.35	389	3.19	404	3.07
[Ni(2Tz(Ph)2Tz)Cl] (**2**)	2.28	3.06	437	2.84	454	2.73
[Ni(2Btz(Ph)2Btz)Cl] (**3**)	1.80	2.91	443	2.80	466	2.66
[Ni(PyPhPy)Br] [g]	2.37	3.09 [c]	433	2.86	468	2.65
[Ni(4Tz(Ph)Py)Br] (**4**)	2.41	3.08	416	2.98	403	3.08
[Ni(2Tz(Ph)Py)Br] (**5**)	2.29	3.08	430	2.88	428	2.90
[Ni(2Btz(Ph)Py)Br] (**6**)	2.02	2.96	421	2.95	444	2.79

[a] $\Delta E_{\text{redox(exp.)}} = \Delta(E_{\text{Ox-1}}–E_{\text{Red-1}})$ from cyclic voltammetry (full data in Table S7, Supplementary Materials). [b] DFT-calculated HOMO and LUMO energies. [c] Experimental long-wavelength absorption maxima (full data in Table S8, Supplementary Materials). [d] Optical band gap derived from long-wavelength maxima (full data in Table S8, Supplementary Materials). [e] TD-DFT-calculated maxima from convoluted spectra. [f] TD-DFT-calculated optical band gap. [g] From ref. [20].

2.4. UV-Vis Absorption Spectroscopy and TD-DFT Calculated Transitions

The UV-vis absorption spectra of the complexes are characterized by intense absorptions in the UV range from 200 to 350 nm (6.1 to 3.54 eV) (Figures 4 and S85, data in Table S8).

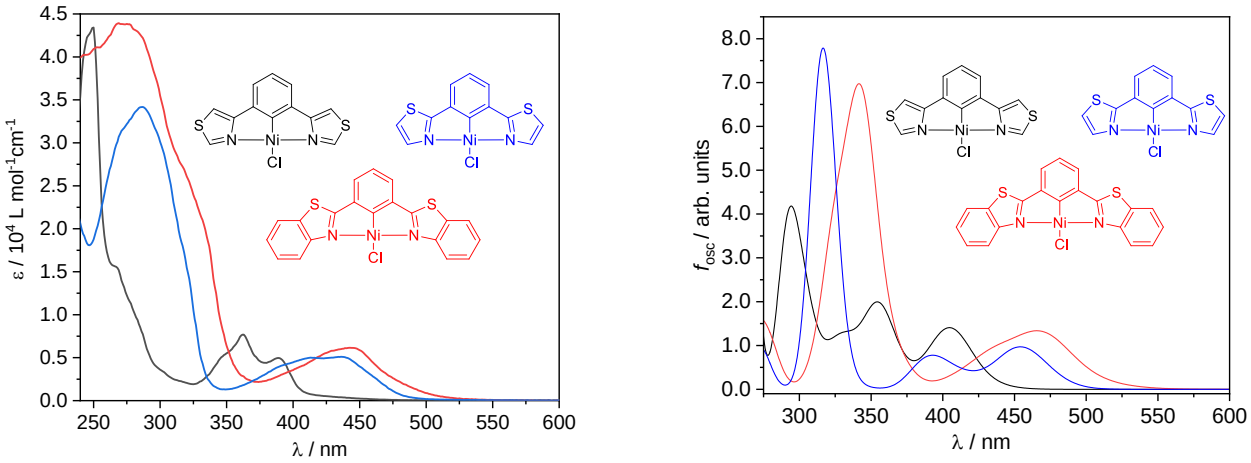

Figure 4. Experimental (left) and DFT calculated (right) UV-vis absorption spectra of symmetric complexes **1** [Ni(4Tz(Ph)4Tz)Cl] (black), **2** [Ni(2Tz(Ph)2Tz)Cl] (blue), and **3** [Ni(2Btz(Ph)2Btz)Cl] (red) in THF at room temperature.

Based on comparison with the recently reported C(Ph)^N(Py)^N(Tz) Pd(II) and Pt(II) complexes [40–42], we can assign them to ligand-centered π–π* transitions. Our TD-DFT calculations on the complexes **2** and **6** (details in Figures S86 and S87, Supplementary Materials) essentially agree with this but also show small Ni and Br contributions to the transitions in this energy range.

The energies of the long-wavelength absorption maxima in the range 350 to 550 nm are highest for the symmetric 4Tz complex **1** (389 nm) and lowest for the bis-2BTz complex **3** (443 nm) (Table 1). The symmetric complexes thus reveal large differences between the 4Tz (**1**) and the 2(B)tz (**2** and **3**) derivatives, in agreement with the different LUMO compositions and energies discussed above. In the non-symmetric complexes, the long-wavelength bands are quite uniform and show only a small difference between the 4Tz (**4**) and the 2Btz (**6**) derivatives (Figure S85), in line with predominantly the Ph(Py) unit contributing essentially to the LUMO in all three cases. The TD-DFT calculations show also mixed ligand/Ni/Br contributions for the long-wavelength transitions, but with generally larger Ni and Br contributions compared with the transitions in the UV range. Overall, we would thus assign the long-wavelength transitions to be of mixed ligand-centered (LC(π–π*))/metal-to-ligand(Ni-π*) charge transfer (MLCT) character. Generally, the TD-DFT-calculated UV-vis spectra (Figures 4 and S85, right) agree with the experimental spectra and data (Table S8, Supplementary Materials).

The complexes [Ni(Py(Ph)Py)X] (X = Cl or Br) show long-wavelength absorptions at 437 and 433 nm. They are markedly lower in energy than the bands of the 4Tz complexes **1** and **4**, in the same range as those of the 2Tz derivatives **2** and **5**, while the 2Btz complexes **3** and **6** show markedly red-shifted long-wavelength absorptions (Table 1). This correlates well with the marked differences in the DFT-calculated HOMO-LUMO gap energies and compositions as well as the electrochemical gaps $\Delta E_{\text{redox(exp.)}}$ of the complexes containing 4Tz, 2Tz, Py, and 2Btz moieties (Table 1) as discussed above with the electron-accepting capacity increasing along the series 4Tz < Py < 2Tz < 2Btz.

2.5. Negishi-Type C–C Cross-Coupling Catalysis

The six new Ni(II) complexes with thiazole-containing N^C^N or N^C^N′ ligands were studied in C–C cross-coupling catalysis of the Negishi-type in comparison with the parent [Ni(Py(Ph)Py)X] (X = Cl or Br) derivatives, using two different model reactions (Scheme 4).

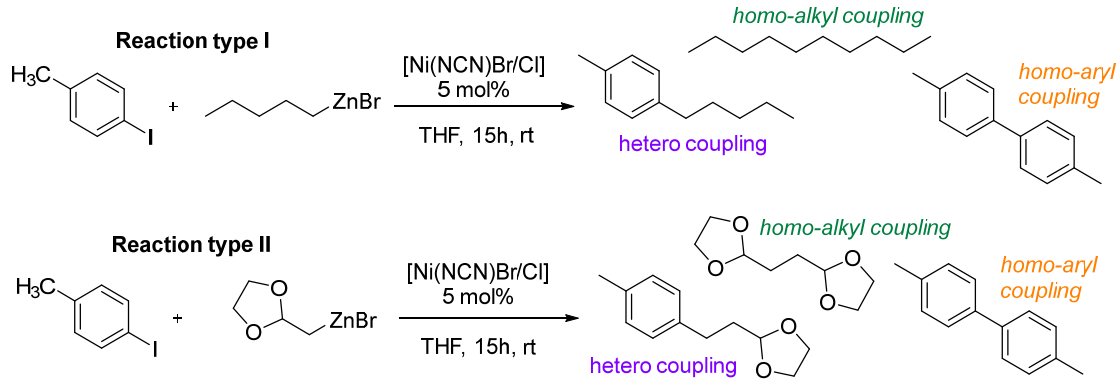

Scheme 4. Reaction type I for Negishi-type cross-coupling catalysis using thiazole-containing Ni(II) complexes. Color code for type of coupling is the same as in Figure 5.

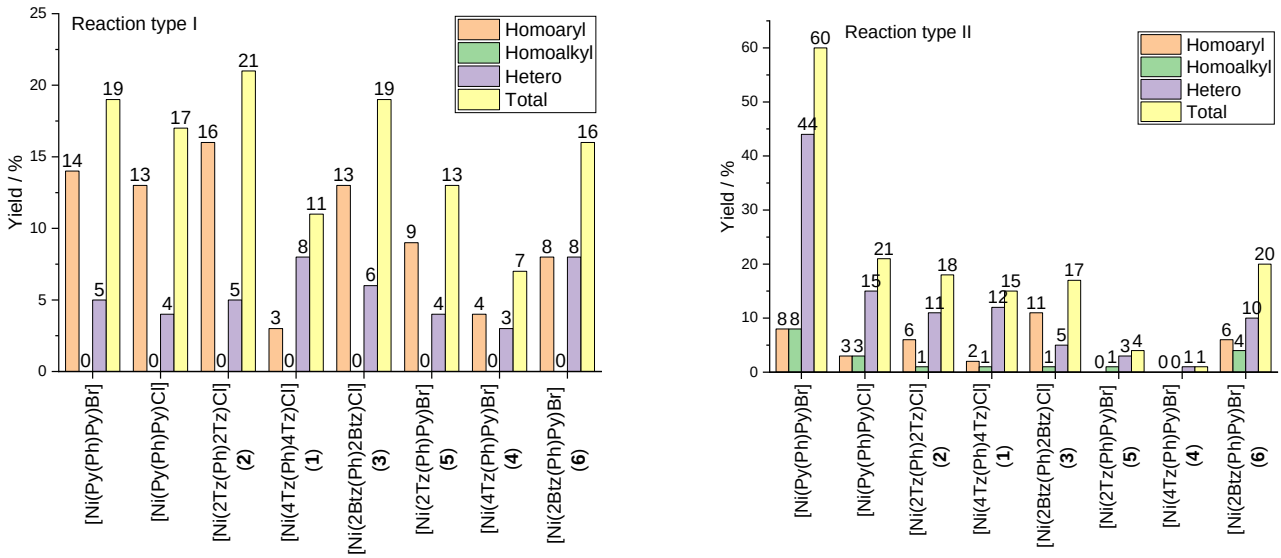

Figure 5. Yields for C–C cross-coupling catalysis for reaction type I (left) and reaction type II (right) using thiazole-containing Ni(II) complexes in comparison to dipyridylbenzene derivatives [Ni(PyPhPy)X] (X = Cl or Br).

The total yields range from 1 to 21% for reaction I and II, with the exception of [Ni(Py(Ph)Py)Br], which reached 60% for the type II reaction (Figure 5). For this complex, the ratio of the desired hetero-coupling to the unwanted homo-alkyl or homo-aryl coupling is the best with 1:0.36 (complete data in Tables S9 and S10, Supplementary Materials).

From the new thiazole-containing complexes, the symmetric 2Tz derivative **2** performed best for reaction type I and type II, followed by the symmetric 2BTz complex **3** and the non-symmetric 2Btz(Ph)Py derivative **6**. They have in common that the electrochemical reduction is facilitated compared with the complexes **1** and **4**, which means more facile production and probably higher stability of the active "reduced" [Ni(N^C^N)(solv)] catalysts, as an important part of the accepted mechanism for the Negishi-type of cross-coupling reactions based on Ni(II) precatalysts. However, following the same argument, the complex **5** should also show good performance. This is true for reaction type I, but not for reaction type II. As the oxidation potentials are rather invariant within our series of complexes, the stability of the Ni(III) state, which is another important species in Negishi-type reactions, is also invariant. Thus, from this side, we cannot explain the differences in C–C coupling efficiency. As the herein shown results are backed by repeated experiments, we are, at the moment, not able to explain the markedly superior performance of [Ni(Py(Ph)Py)Br] over the thiazole-containing complexes **1** to **6** in reaction type II and the failure of complex **5** in

the same reaction. Therefore, we will compare the new complexes **1** to **6** with the Py(Ph)Py derivative using other substrates in the near future, hopefully allowing more insight and also an estimate of the possible substrate scope.

In our prior paper [14], we noted: "We tentatively ascribe the huge difference in terms of selectivity for reaction I vs. reaction II to the possibility for Zn to form a chelate binding using the dioxane function in reaction II, thus tuning its reactivity." Similar phenomena have been reported previously [52–54]. Further, the role of the different halides might go beyond that of being a more or less suitable leaving group. Salt byproducts are known to play a critical role in Negishi-type cross-coupling reactions [55,56].

When comparing the results for the Ni(NCN) configured complex with the overall best performance, [Ni(Py(Ph)Py)Br] with the previously reported Ni(CNN) derivatives of the type [NiPhbpy)X] (X = F, Cl, Br, I), the Phbpy complexes perform generally better in both yields (43 to 64%) and selectivity [14] and the differences between reaction type I and type II were minor. Substitution on the Phbpy core leads to lower reactivity in some cases but higher reactivity in other cases, with the 3-MeO-Phbpy derivative reaching 72% [14]. Thus, the replacement of one or two pyridines in the [Ni(Py(Ph)Py)Br] complex did not increase activity, and neither was the question of symmetry or non-symmetry of importance. And the Ni(CNN) derivatives seem to have superior activities when comparing these two studies.

A strong dependence on the ligand in Ni-catalyzed Negishi-type coupling has been frequently observed. The deaminative Csp^3–Csp^3 coupling reaction of phenyl-ethyl-N-(2,4,6-trimethyl)pyridinium with ((1,3-dioxolan-2-yl)ethyl)zinc(II) bromide, using [$Ni(acac)_2$] or [$NiCl_2$(DME)] along with α-diimine ligands (bpy or terpy derivatives) gave yields ranging from 14 to 81% [57]. Optimized catalysts and reaction methods allowed enantioselective Csp^2-Csp^3 coupling under reductive conditions in yields around 90% under reductive conditions in a benchmark study [58].

3. Materials and Methods

3.1. Materials

The commercially available chemicals are listed in Section S1.1 in the Supplementary Materials. The synthesis and characterization of the N^C(H)^N′ and N^C(Cl)^N protoligands is reported in the Supplementary Materials Section S1.2.

3.2. Syntheses

3.2.1. Synthesis of [$Ni(COD)_2$]

An amount of 3.92 g $Ni(acac)_2$ (15 mmol, 1.0 eq.) was vacuum dried and suspended in 60 mL THF under an inert atmosphere. An amount of 7.04 g 1,5-cyclooctadiene (65 mmol, 4.3 eq.) and a solution of ca. 50 mL DIBAl-H in hexanes (0.95 M, 48 mmol, 3.2 eq.) were added and stirred for 2 h at room temperature. After addition of 100 mL Et_2O, the mixture was stored at −18 °C overnight. The next day, the liquid phase was decanted and the remaining solid was washed with 50 mL acetone and twice with 50 mL *n*-heptane. After drying under reduced pressure, 0.82 g (3.0 mmol, 20%) yellow crystals were obtained, which were used for following syntheses without further characterization.

3.2.2. Synthesis of the Symmetric Complexes [Ni(N^C^N)Cl]—General Procedure

Under inter conditions, 0.27 g [$Ni(COD)_2$] (1.0 mmol, 1.0 eq.) was suspended in THF (10 mL) and ligand L_{Symm}–Cl (1.2 mmol, 1.2 eq.) was added. The reaction was stirred overnight and then treated with 20 mL *n*-pentane to precipitate the products. After filtration, the remaining solids were washed with 2 × 20 mL *n*-pentane and dried under reduced pressure.

[Ni(4Tz(Ph)4Tz)Cl] (1). Yield: 0.33 g (0.99 mmol, 99%) yellow solid. $C_{12}H_7ClN_2NiS_2$ (M = 337.47 g mol^{-1}). ^{1}H NMR: (300 MHz, DMSO-d$_6$) δ [ppm] = 9.10 (d, *J* = 1.3 Hz, 2H, H7), 8.00 (d, *J* = 1.00 Hz, 2H, H6), 7.34 (d, *J* = 7.6 Hz, 2H, H3), 7.16 (t, *J* = 7.5 Hz, 1H, H2). EI-MS(+): *m*/*z* = 336 (60%) [M]$^+$, 301 (100%) [M–Cl]$^+$, 274 (10%) [M–Cl–2(CH)$_{4Tz}$]$^+$, 244 (10%) [M–NiCl+H]$^+$, 216 (5%) [M–NiCl–2(CH)$_{4Tz}$]$^+$ or [M–4Tz]$^+$, 189 (5%) [M–NiCl–2(CNH)$_{4Tz}$]$^+$. Elemental anal. found (calc.): C, 42.72 (42.71); H, 2.10 (2.09); N, 8.33 (8.30); S, 18.96 (19.00).
[Ni(2Tz(Ph)2Tz)Cl] (2). Yield: 0.28 g (0.82 mmol, 82%) yellow solid. $C_{12}H_7ClN_2NiS_2$ (M = 337.47 g mol^{-1}). ^{1}H NMR: (300 MHz, DMSO-d$_6$) δ [ppm] = 7.76 (s, 4H, H6, H7), 7.52 (d, *J* = 7.6 Hz, 2H, H3), 7.19 (t, *J* = 7.6 Hz, 1H, H2). EI-MS(+): *m*/*z* = 336 (40%) [M]$^+$, 301 (100%) [M–Cl]$^+$, 244 (10%) [M–NiCl+H]$^+$, 216 (5%) [M–NiCl–2(CH)$_{2Tz}$]$^+$ or [M–2Tz]$^+$, 211 (30%) [M–NiCl–S$_{2Tz}$]$^+$, 187 (15%) [M–NiCl–2(NCH)$_{2Tz}$]$^+$. Elemental anal. found (calc.): C, 42.76 (42.71); H, 2.01 (2.09); N, 8.28 (8.30); S, 18.81 (19.00).
[Ni(2Btz(Ph)2Btz)Cl] (3). The reaction gave 0.44 g (0.99 mmol, 99%) orange solid. $C_{20}H_{11}ClN_2NiS_2$ (M = 437.59 g mol^{-1}). ^{1}H NMR: (300 MHz, DMSO-d$_6$) δ [ppm] = 8.31–8.22 (m, 4H, H3, H10), 8.18 (d, *J* = 8.2 Hz, 1H, H7), 7.77 (t, *J* = 7.8 Hz, 1H, H2), 7.63 (t, *J* = 7.99 Hz, 2H, H8), 7.56 (t, *J* = 7.5 Hz, 2H, H9). EI-MS(+): *m*/*z* 435 (1%) [M]$^+$, 401 (42%) [M–Cl]$^+$, 378 (100%) [M–Ni]$^+$, 344 (80%) [M–Ni–S$_{2Btz}$]$^+$, 311 (20%) [M–NiCl–S$_{2Btz}$]$^+$, 267 (5%) [M–Cl–2Btz]$^+$, 235 (5%) [M–Cl–2Btz–S$_{2Btz}$]$^+$, 189 (20%) [M–NiCl–PhNS$_{2Btz}$]$^+$. Elemental anal. found (calc.): C, 54.95 (54.90); H, 2.54 (2.53); N, 6.43 (6.40); S, 14.81 (14.85).

3.2.3. Synthesis of the Non-Symmetric Complexes [Ni(NˆCˆN′)Br]—General Procedure

In an inert flask with a water trap filled with molecular sieve (3 Å), anhydrous 0.28 g $NiBr_2$ (1.3 mmol, 1.3 eq.), 0.10 g KOAc (1.0 mmol, 1.0 eq.) and 0.14 g K_2CO_3 (1.0 mmol, 1.0 eq.) were dried for 1 h in vacuum at 170 °C. Then, 1.0 mmol, 1.0 eq. of HL and dry *p*-xylene (200 mL) were added and the reaction was heated under reflux for 72 h and cooled down to ambient temperature. The reaction mixture was filtered off, the precipitate was washed with 50 mL *p*-xylene, and the solvent from the filtrate was removed under reduced pressure. The product could be further purified through recrystallization out of a THF/*n*-pentane mixture.
[Ni(4Tz(Ph)Py)Br] (4). Yield: 0.29 g (0.77 mmol, 77%) dark yellow crystals. $C_{14}H_9BrN_2NiS$ (M = 375.90 g/mol). ^{1}H NMR: (300 MHz, DMSO-*d*$_6$) δ [ppm] = 9.27 (d, *J* = 1.9 Hz, 1H, H14), 8.82 (d, *J* = 5.5 Hz, 1H, H2), 8.01 (t, *J* = 7.6 Hz, 2H, H4, H13), 7.87 (d, *J* = 7.4 Hz, 1H, H5), 7.46 (d, *J* = 7.5 Hz, 1H, H8), 7.39 (d, *J* = 7.5 Hz, 1H, H10), 7.30 (t, *J* = 6.9 Hz, 1H, H3), 7.18 (t, *J* = 7.5 Hz, 1H, H9). EI(+)-MS (70 eV) *m*/*z* = 375 (2%) [M]$^+$, 366 [M–CH$_{4Tz}$]$^+$, 331 (15%) [M–(SCH)$_{4Tz}$]$^+$, 314 (25%) [M–(S(CH)$_2$)$_{4Tz}$]$^+$, 294 (5%) [M–Br]$^+$, 277 (15%) [M–4Tz–C$_{Ph}$]$^+$, 255 (20%) [M–Br–(C$_3$H$_3$)$_{Py}$]$^+$, 251 (100%) [M–Br–(SCH)$_{4Tz}$]$^+$, 238 (100%) [M–NiBr]$^+$. Elemental anal. found (calc.): C, 44.75 (44.73); H, 2.44 (2.41); N, 7.40 (7.45); S, 8.52 (8.53).
[Ni(2Tz(Ph)Py)Br] (5). Yield: 0.24 g (0.64 mmol, 64%) of orange-brown crystals. $C_{14}H_9BrN_2NiS$ (M = 375.90 g/mol). ^{1}H NMR: (300 MHz, DMSO-*d*$_6$): δ [ppm] = 8.69 (d, *J* = 4.5 Hz, 1H, H2), 8.05 (t, *J* = 7.5 Hz, 1H, H4), 7.89 (d, *J* = 7.6 Hz, 1H, H5), 7.80 (d, *J* = 3.4 Hz, 1H, H14), 7.69 (d, *J* = 3.2 Hz, 1H, H13), 7.52 (d, *J* = 7.3 Hz, 1H, H8), 7.43 (d, *J* = 7.5 Hz, 1H, H10), 7.30 (t, *J* = 6.4 Hz, 1H, H3), 7.17 (t, *J* = 7.6 Hz, 1H, H9). EI(+)-MS (70 eV) *m*/*z* = 376 (10%) [M]$^+$, 343 (1%) [M–S$_{2Tz}$]$^+$, 320 (25%) [M–(S(CH)$_2$)$_{2Tz}$]$^+$, 289 (35%) [M–(2Tz)]$^+$, 252 (100%) [NiBrPy+(C$_3$H)$_{Ph}$]$^+$, 204 (5%) [M–Ni–Br–S$_{2Tz}$]$^+$, 192 (15%) [M–Ni–Br–(CHS)$_{2Tz}$]$^+$, 181 (5%) [M–Ni–Br–(S(CH)$_2$)$_{2Tz}$]$^+$. Elemental anal. found (calc.): C, 44.75 (44.73); H, 2.40 (2.41); N, 7.43 (7.45); S, 8.63 (8.53).
[Ni(2Btz(Ph)Py)Br] (6). Yield: 0.20 g (0.47 mmol, 47%) deep orange powder. $C_{18}H_{11}BrN_2NiS$ (M = 425.96 g/mol). ^{1}H NMR: (300 MHz, CD_2Cl_2) δ [ppm] = 9.20 (s, 1H, H2), 9.03 (s, 1H, H17), 7.77–7.60 (m, 2H, H4, H14), 7.38 (t, *J* = 7.2 Hz, 2H, H3, H16), 7.28 (t, *J* = 7.0 Hz, 1H, H15), 7.22–7.12 (m, 2H, H8, H10), 7.03–6.94 (m, 2H, H5, H9). Sample not stable in dry DMSO-d$_6$.

EI(+)-MS (70 eV) m/z = 424 (1%) $[M]^+$, 394 (1%) $[M–S_{2Btz}]^+$, 366 (10%) $[M–(S(CH)_2)_{2Btz}]^+$, 347 (10%) $[M–Ph_{2Btz}]^+$, 345 (10%) $[M–Br]^+$, 332/331 (20%) $[M–Br–(CH)_{Py/Ph/2Btz}]^+$, 301 (100%) $[NiBrPyPh+C_{2Btz}]^+$, 287 (40%) $[M–NiBr]^+$, 275 (5%) $[M–NiBrC]^+$, 255 (10%) $[M–NiBrS_{2Btz}]^+$. Elemental anal. found (calc.): C, 50.41 (50.76); H, 2.61 (2.60); N, 6.51 (6.58); S, 7.53 (7.53).

3.3. Instrumentation

^1H, ^{13}C, and correlation spectra were recorded on a Bruker Avance II 300 MHz (^1H: 300 MHz, ^{13}C: 75 MHz) equipped with a L.T. BBO ATM 5 mm probe head with z-gradient coil (Bruker, Rheinhausen, Germany) and on *a Bruker* Avance III 500 MHz (^1H: 500 MHz, ^{13}C: 125 MHz) equipped with a TCI prodigy 5 mm probe head with z-gradient coil (Bruker, Rheinhausen, Germany). Chemical shifts were relative to TMS (^1H, ^{13}C). UV–vis absorption spectra were recorded on a Varian Cary 05E spectrophotometer (Varian Medical Systems, Darmstadt, Germany). Elemental analyses were obtained using a HEKAtech CHNS EuroEA 3000 analyzer (HEKAtech, Wegberg, Germany). EI-MS spectra in the positive mode were measured using a Thermo Scientific Exactive GC Orbitrap Analyser mass spectrometer (Thermo Fisher Scientific GmbH, Dreieich, Germany). Electrochemical measurements were carried out in 0.1 M n-Bu_4NPF_6 solution in THF (tetrahydrofuran) using a three-electrode configuration (glassy carbon electrode, Pt counter electrode, Ag/AgCl reference) and a Metrohm Autolab PGSTAT30 or µStat400 potentiostat (Metrohm, Filderstadt, Germany). The potentials were referenced against the ferrocene/ferrocenium redox couple as internal standard.

3.4. Single Crystal Structure Analysis by X-Ray Diffractometry (scXRD)

The measurements were performed at 170(2) K using a Bruker D8 Venture, including a Bruker Photon 100 CMOS detector using Mo-Kα radiation (λ = 0.71073 Å) (Bruker, Rheinhausen, Germany). The crystal data was collected using APEX3 v2015.5-2 [59]. The structures were solved by dual space methods using SHELXT [60,61] and refinement was carried out with SHELXL 2017 employing full-matrix least-squares methods on $F_0^2 \geq 2\sigma(F_0^2)$ [61,62]. The non-hydrogen atoms were refined with anisotropic displacement parameters without any constraints. The hydrogen atoms were included by using appropriate riding models. Data of the structure solutions and refinements can be obtained under the accession numbers CCDC 2277899 for **1**. 2277904 for **2**, 2277902 for **3**, 2277919 for **4**, 2277912 for **5**, and 2277925 for **6**·0.5THF free of charge at https://www.ccdc.cam.ac.uk/structures/ or from the Cambridge Crystallographic Data Centre, 12 Union Road, Cambridge, CB2 1EZ UK (fax: +44-1223 336033 or e-mail: deposit@ccdc.cam.ac.uk).

3.5. Computational Details

All DFT calculations were performed using ORCA 5.0.2 [63,64]. def2-TZVP basis sets were used for all atoms [65]. The geometry of all compounds was optimized at the BP86 level of theory, using *Grimme's* D3 dispersion correction and the conductor-like polarizable continuum model (CPCM) parametrized for THF as an approximate solvation model [66–71]. The geometry optimizations were followed up with numerical frequency calculations to confirm the energetic minimum nature of the optimized structure as indicated by the absence of imaginary modes. On the optimized geometries, single-point and TD-DFT calculations were performed using the TPSSh functional, *Grimme's* D3 dispersion correction and CPCM parametrized for THF [68–72]. For the TD-DFT calculations of absorption spectra, 40 roots (transitions) for singlets and triplets each were included for each complex. Broadened spectra were obtained using the orca_mapspc module with 2000 cm^{-1} full width at half maximum band broadening. Orbital isosurfaces and TD-DFT difference densities were extracted from the single-point calculations using the ORCA module orca_plot and plotted with the visualization

software CHEMCRAFT V1.8 at an isovalue of 0.04 for molecular orbitals and 0.001 for difference densities [73].

3.6. Catalysis Experiments

An amount of 0.109 g (0.5 mmol) of 4-iodotoluene was dissolved in THF (5 mL). Then, 1 mL of zinc reagent (0.5 mmol, 0.5 M solution in THF) was added into the solution. An amount of 81 mg (0.5 mmol, 1 eq. for 100% conversion) hexamethylbenzene was added as the internal standard. The response factor for 1-methyl-4-pentylbenzene was 0.985 and for 2-(4-methylphenethyl)-1-3-dioxane was 0.794. Then, 5% mmol of Ni(II) catalyst was added into the solution while stirring. The stirring was stopped after 15 h by addition of H_2O (2 mL) and sit for 2 h. A volume of 1 mL of the organic layer was filtered through an alumina plug and washed with 10 mL of MeOH to reach a conc. of 1 mg/mL for the GC-MS analysis.

3.7. GC-MS Analysis

The GC-MS measurements were performed with a SHIMADZU QP2010 Ultra device and evaluated using GCMS Postrun Analysis software by SHIMADZU.

4. Conclusions

In the six NˆCˆN cyclometalated Ni(II) complexes [Ni(NˆCˆN)Cl] or [Ni(NˆCˆN′)Br] with symmetric NˆCˆN or non-symmetric NˆCˆN′ ligands the substitution of the peripheral N-groups from pyridine (Py) to 4-thiazole (4Tz), 2-thiazole (2Tz), and 2-benzothiazole (2Btz) complemented the previously reported complexes with di(2-pyridyl)phenide ligands [Ni(Py(Ph)Py)X] X = Cl or Br. A remarkable difference was found for the synthesis conditions. While the non-symmetric [Ni(NˆCˆN′)Br] were synthesized from $NiBr_2$ and NˆCHˆN′ protoligands through the established base-assisted nickelation, the symmetric [Ni(NˆCˆN)Cl] were not received through this procedure. Instead they were synthesized from the NˆC(Cl)ˆN protoligands and [Ni(COD)$_2$] (COD = 1,5-cyclooctadiene). Compared to Py, the introduction of 4Tz on both sides shifted the first reduction to quite negative values and the electrochemical gap $\Delta E_{exp.} = E_{ox} – E_{red}$ and the long wavelength UV-vis absorption maxima to higher energies. In contrast, introduction of 2Tz and 2Btz led to facilitated reduction and shifts to lower energies. When introducing only one 4Tz or 2Tz as peripheral groups, the remaining PhPy moiety dominates the electronic properties, and thus electrochemistry and photophysics are very similar to the Py(Ph)Py systems. The 2Btz moieties dominate the character of the frontier molecular orbitals for both mono and di-substituted ligands, as DFT calculations show. TD-DFT calculations show very mixed character for the transitions underlying the UV-vis absorption spectra. Overall, the energy of these absorptions correlates very well with the first reduction potentials. Negishi-type C–C cross-coupling reactions using the six thiazole-containing complexes gave total yields ranging from 1 to 21% compared with 60% for the [Ni(Py(Ph)Py)Br] derivative. The reactivities correlate reasonably with the first reduction potentials in keeping with the idea that the reduced complexes [Ni(NˆCˆN)(solv)] (solv = solvent molecule) that were produced from reduction of the parent [Ni(NˆCˆN)X] complexes and rapid X^- cleavage are the active catalysts. This is regardless of the conclusion from DFT that the reduces species should not be described as Ni(I) species but rather as Ni(II) complexes containing radical anionic $NˆCˆN^{•-}$ ligands. Facilitated reduction (E around −2 or higher) for the 2Tz and 2Btz-containing complexes goes generally along with improved performance, regardless of the loci of the added electron. This makes these thiazole-containing complexes interesting candidates for such catalysis on substrates which are sensitive to very negative potentials.

Supplementary Materials: The following supporting information can be downloaded at: https://www.mdpi.com/article/10.3390/inorganics13020041/s1. The materials contain S1. Synthesis and analytical data. S2. Supplementary Figures (NMR spectra, EI(+)-MS, crystal and molecular structures from single-crystal X-ray diffraction, cyclic voltammograms, DFT-calculated frontier molecular orbitals and energies, experimental and DFT-calculated UV-vis absorption spectra). S3. Supplementary Tables (crystal data, selected bond parameters from experiment and DFT calculations, redox potentials, UV-vis absorption maxima, yields for C–C cross-coupling reactions).

Author Contributions: The experimental work was carried out by L.K. and J.S., except the catalysis that was performed by L.K. under the supervision of D.A.V. The computational work was done by R.J. The original draft was written by R.J. and A.K.; A.K., R.J. and D.A.V. revised the original draft. All authors have read and agreed to the published version of the manuscript.

Funding: We acknowledge funding from the Cusanuswerk e.V. (L.K.) and Studienstiftung des Deutschen Volkes e.V. (R.J.). D.A.V. thanks the U.S. National Science Foundation (CHE-2153730) for support of this work.

Data Availability Statement: The data presented in this study are available on request from the corresponding author.

Acknowledgments: Sean Sebastian, Department of Chemistry and Biochemistry, University of Cologne is acknowledged for help with the crystal structure solution.

Conflicts of Interest: The authors declare that they have no known competing financial interests or personal relationships that could have appeared to have influenced the work reported in this paper.

References

1. Johansson Seechurn, C.C.C.; Kitching, M.O.; Colacot, T.J.; Snieckus, V. Palladium-Catalyzed Cross-Coupling: A Historical Contextual Perspective to the 2010 Nobel Prize. *Angew. Chem. Int. Ed.* **2012**, *51*, 5062–5085. [CrossRef] [PubMed]
2. Diccianni, J.; Lin, Q.; Diao, T. Mechanisms of Nickel-Catalyzed Coupling Reactions and Applications in Alkene Functionalization. *Acc. Chem. Res.* **2020**, *53*, 906–919. [CrossRef] [PubMed]
3. Ogishi, S. (Ed.) *Nickel Catalysis in Organic Synthesis—Methods and Reactions*; Wiley/VCH: Weinheim, Germany, 2019.
4. Phapale, V.B.; Cárdenas, D.J. Nickel-catalysed Negishi cross-coupling reactions: Scope and mechanisms. *Chem. Soc. Rev.* **2009**, *38*, 1598–1607. [CrossRef] [PubMed]
5. Han, F.-S. Transition-metal-catalyzed Suzuki–Miyaura cross-coupling reactions: A remarkable advance from palladium to nickel catalysts. *Chem. Soc. Rev.* **2013**, *42*, 5270–5298. [CrossRef]
6. Pawlak, M.; Drzezdzon, J.; Jacewicz, D. The greener side of polymers in the light of d-block metal complexes as Precatalysts. *Coord. Chem. Rev.* **2023**, *484*, 215122. [CrossRef]
7. Zhang, R.; Gao, R.; Gou, Q.; Lai, J.; Li, X. Recent Advances in the Copolymerization of Ethylene with Polar Comonomers by Nickel Catalysts. *Polymers* **2022**, *14*, 3809. [CrossRef]
8. Lee, B.C.; Liu, C.-F.; Lin, L.Q.H.; Yap, K.Z.; Song, N.X.; Ko, C.H.M.; Chan, P.H.; Koh, M.J. *N*-Heterocyclic carbenes as privileged ligands for nickel-catalysed alkene functionalization. *Chem. Soc. Rev.* **2023**, *52*, 2946–2991. [CrossRef] [PubMed]
9. Kranthikumar, R. Recent Advances in $C(sp^3)-C(sp^3)$ Cross-Coupling Chemistry: A Dominant Performance of Nickel Catalysts. *Organometallics* **2022**, *41*, 667–679. [CrossRef]
10. Yi, L.; Ji, T.; Chen, K.-Q.; Chen, X.-Y.; Rueping, M. Nickel-Catalyzed Reductive Cross-Couplings: New Opportunities for Carbon–Carbon Bond Formations through Photochemistry and Electrochemistry. *CS Chem.* **2022**, *4*, 9–30. [CrossRef]
11. Zhu, C.; Yue, H.; Jia, J.; Rueping, M. Nickel-Catalyzed C-Heteroatom Cross-Coupling Reactions under Mild Conditions via Facilitated Reductive Elimination. *Angew. Chem. Int. Ed.* **2021**, *60*, 17810–17831. [CrossRef]
12. Dudkina, Y.B.; Fayzullin, R.R.; Lyssenko, K.A.; Gubaidullin, A.T.; Kholin, K.V.; Levitskaya, A.I.; Balakina, M.Y.; Budnikova, Y.H. Cyclometalated Nickel Complexes as Key Intermediates in $C(sp^2)-H$ Bond Functionalization: Synthesis, Catalysis, Electrochemical Properties, and DFT Calculations. *Organometallics* **2019**, *38*, 1254–1263. [CrossRef]
13. Mousa, A.H.; Chakrabarti, K.; Isapour, G.; Bendix, J.; Wendt, O.F. Enhancing the Stability of Aromatic PCN Pincer Nickel Complexes by Incorporation of Pyridine as the Nitrogen Side Arm. *Eur. J. Inorg. Chem.* **2020**, *2020*, 4270–4277. [CrossRef]
14. Vogt, N.; Sandleben, A.; Kletsch, L.; Schäfer, S.; Chin, M.T.; Vicic, D.A.; Hörner, G.; Klein, A. On the Role of the X Coligands in Cyclometalated [Ni(Phbpy)X] Complexes (HPhbpy = 6-phenyl-2,2′-bipyridine). *Organometallics* **2021**, *40*, 1776–1785. [CrossRef]
15. Gilbert, M.M.; Trenerry, M.J.; Longley, V.R.; Castro, A.J.; Berry, J.F.; Weix, D.J. Ligand−Metal Cooperation Enables Net Ring-Opening C−C Activation/Difunctionalization of Cyclopropyl Ketones. *ACS Catal.* **2023**, *13*, 11277–11290. [CrossRef] [PubMed]

16. Quirós, M.T.; Collado-Sanz, D.; Buñuel, E.; Cárdenas, D.J. Ligand-Controlled Electron Structure of Catalytically Active Ni Complexes. *J. Phys. Chem. A* **2018**, *122*, 2250–2257. [CrossRef]
17. An, L.; Xu, C.; Zhang, X. Highly selective nickel-catalyzed *gem*-difluoropropargylation of unactivated alkylzinc reagents. *Nat. Commun.* **2017**, *8*, 1460. [CrossRef] [PubMed]
18. Ciszewski, J.T.; Mikhaylov, D.Y.; Holin, K.V.; Kadirov, M.K.; Budnikova, Y.H.; Sinyashin, O.; Vicic, D.A. Redox Trends in Terpyridine Nickel Complexes. *Inorg. Chem.* **2011**, *50*, 8630–8635. [CrossRef] [PubMed]
19. Wong, Y.-S.; Tang, M.-C.; Ng, M.; Yam, V.W.-W. Toward the Design of Phosphorescent Emitters of Cyclometalated Earth-Abundant Nickel(II) and Their Supramolecular Study. *J. Am. Chem. Soc.* **2020**, *142*, 7638–7646. [CrossRef]
20. Kletsch, L.; Hörner, G.; Klein, A. Cyclometalated Ni(II) Complexes [Ni(N^C^N)X] of the Tridentate 2,6-di(2-pyridyl)phen-ide Ligand. *Organometallics* **2020**, *39*, 2820–2829. [CrossRef]
21. Kletsch, L.; Jordan, R.; Köcher, A.S.; Buss, S.; Strassert, C.A.; Klein, A. Photoluminescence of Ni(II), Pd(II), and Pt(II) Complexes [M(Me_2dpb)Cl] Obtained from C–H Activation of 1,5-Di(2-pyridyl)-2,4-dimethylbenzene (Me_2dpbH). *Molecules* **2021**, *26*, 5051. [CrossRef]
22. Cardenas, D.J.; Echavarren, A.M.; Ramirez de Arellano, M.C. Divergent Behavior of Palladium(II) and Platinum(II) in the Metalation of 1,3-Di(2-pyridyl)benzene. *Organometallics* **1999**, *18*, 3337–3341. [CrossRef]
23. Soro, B.; Stoccoro, S.; Minghetti, G.; Zucca, A.; Cinellu, M.A.; Manassero, M.; Gladiali, S. The first pincer-aryl [M–(NCN)] complexes {M = Pd(II); Pt(II)} with chiral pyridine donors: Synthesis and catalytic activity in C–C bond formation. *Inorg. Chim. Acta* **2006**, *359*, 1879–1888. [CrossRef]
24. Soro, B.; Stoccoro, S.; Minghetti, G.; Zucca, A.; Cinellu, M.A.; Gladiali, S.; Manassero, M.; Sansoni, M. Synthesis of the First C-2 Cyclopalladated Derivatives of 1,3-Bis(2-pyridyl)benzene. Crystal Structures of [Hg(N-C-N)Cl], [Pd(N-C-N)Cl], and [Pd_2(N-C-N)$_2$(μ-OAc)]$_2$[Hg_2Cl_6]. Catalytic Activity in the Heck Reaction. *Organometallics* **2005**, *24*, 53–61. [CrossRef]
25. Vogt, N.; Sivchik, V.; Sandleben, A.; Hörner, G.; Klein, A. Direct Base-Assisted C–H Cyclonickelation of 6-Phenyl-2,2′-bipyridine. *Molecules* **2020**, *25*, 997. [CrossRef]
26. Green, K.-A.; Honeycutt, A.P.; Ciccone, S.R.; Grice, K.A.; Baur, A.; Petersen, J.L.; Hoover, J.M. A Redox Transmetalation Step in Nickel-Catalyzed C−C Coupling Reactions. *ACS Catal.* **2023**, *13*, 6375–6381. [CrossRef]
27. Sandleben, A.; Vogt, N.; Hörner, G.; Klein, A. On the Redox Series of Cyclometalated Nickel Complexes $[Ni((R)Ph(R')bpy)Br]^{+/0/-/2-}$ (H–(R)Ph(R′)bpy = substituted 6-phenyl-2,20-bipyridine). *Organometallics* **2018**, *37*, 3332–3341. [CrossRef]
28. Grove, D.M.; van Koten, G.; Ubbels, H.J.C.; Zoet, R. Organonickel(II) Complexes of the Terdentate Monoanionic Ligand *o*,*o*′-Bis[(dimethylamino)methyl]phenyl (N-C-N). Syntheses and the X-ray Crystal Structure of the Stable Nickel(II) Formate [Ni(N-C-N)O_2CH]. *Organometallics* **1984**, *3*, 1003–1009. [CrossRef]
29. Salthouse, R.J.; Sil, A.; Gildea, L.F.; Yufit, D.S.; Williams, J.A.G. Platinum(II) Complexes of Nonsymmetrical NCN-Coordinating Ligands: Unimolecular and Excimeric Luminescence Properties and Comparison with Symmetrical Analogues. *Inorg. Chem.* **2023**, *62*, 12356–12371. [CrossRef] [PubMed]
30. Hruzd, M.; le Poul, N.; Cordier, M.; Kahlal, S.; Saillard, J.-Y.; Achelle, S.; Gauthier, S.; Robin-le Guen, F. Luminescent cyclometalated alkynylplatinum(II) complexes with 1,3-di(pyrimidin-2-yl)benzene ligands: Synthesis, electrochemistry, photophysics and computational studies. *Dalton Trans.* **2022**, *51*, 5546–5560. [CrossRef] [PubMed]
31. Wang, Z.; Turner, E.; Mahoney, V.; Madakuni, S.; Groy, T.; Li, J. Facile Synthesis and Characterization of Phosphorescent Pt(N^C^N)X Complexes. *Inorg. Chem.* **2010**, *49*, 11276–11286. [CrossRef] [PubMed]
32. Develay, S.; Blackburn, O.; Thompson, A.L.; Williams, J.A.G. Cyclometalated Platinum(II) Complexes of Pyrazole-Based, N^C^N-Coordinating, Terdentate Ligands: The Contrasting Influence of Pyrazolyl and Pyridyl Rings on Luminescence. *Inorg. Chem.* **2008**, *47*, 11129–11142. [CrossRef] [PubMed]
33. Yang, B.-Z.; Zhou, X.; Liu, T.; Bai, F.-Q.; Zhang, H.-X. Theoretical Studies on the Electronic Structures and Spectroscopic Properties of a Series of Novel N–C–N-Coordinating Pt(II) Complexes. *Int. J. Quantum Chem.* **2010**, *110*, 1605–1614. [CrossRef]
34. Koo, C.-K.; Wong, K.-L.; Lau, K.-C.; Wong, W.-Y.; Lam, M.H.-W. The Controlled Formation and Cleavage of an Intramolecular d^8–d^8 Pt–Pt Interaction in a Dinuclear Cycloplatinated Molecular "Pivot-Hinge". *Chem.–Eur. J.* **2009**, *15*, 7689–7697. [CrossRef] [PubMed]
35. Lee, S.; Lee, Y.; Kim, K.; Heo, S.; Jeong, D.Y.; Kim, S.; Cho, J.; Kim, C.; You, Y. Twist to Boost: Circumventing Quantum Yield and Dissymmetry Factor Trade-Off in Circularly Polarized Luminescence. *Inorg. Chem.* **2021**, *60*, 7738–7752. [CrossRef]
36. Lorenzo-Aparicio, C.; Moreno-Blázquez, S.; Oliván, M.; Esteruelas, M.A.; Gómez Gallego, M.; García-Álvarez, P.; Cabeza, J.A.; Sierra, M.A. Synthesis, Structure, and Photophysical Properties of Platinum(II) (N,C,N′) Pincer Complexes Derived from Purine Nucleobases. *Inorg. Chem.* **2023**, *62*, 8232–8248. [CrossRef] [PubMed]
37. Li, P.; Zhou, H.-F.; Liu, F.; Hu, Z.-X.; Wang, H.-X. NCN palladium pincer via transmercuration. Synthesis of [2-(2-oxazoliny)-6-(2-pyridyl)] phenylpalladium(II) chloride and its catalytic activity in Suzuki coupling. *Inorg. Chem. Commun.* **2013**, *32*, 78–81. [CrossRef]

38. Li, J.; Mei, Q. Narrow Band Red Phosphorescent Tetradentate Platinum(II) Complexes. Patent WO2018071697, 19 April 2018.
39. Li, J.; Wang, Z.; Turner, E. Preparation of Tridentate Platinum(II) Complexes Useful for Organic Light Emitting Devices. Patent WO2009111299, 11 September 2009.
40. Krause, M.; von der Stück, R.; Brünink, D.; Buss, S.; Doltsinis, N.L.; Strassert, C.A.; Klein, A. Platinum and palladium complexes of tridentate ⁻CˆNˆN (phen-ide)-pyridine-thiazol ligands—A case study involving spectroelectrochemistry, photoluminescence spectroscopy and TD-DFT calculations. *Inorg. Chim. Acta* **2021**, *518*, 120093. [CrossRef]
41. Krause, M.; Friedel, J.; Buss, S.; Brünink, D.; Berger, A.; Strassert, C.A.; Doltsinis, N.L.; Klein, A. Isoelectronic Pt(II) Complexes of Cyclometalating CˆNˆN Ligand with Phenyl/(Benzo)thiophenyl and Pyridine/(Benzo)thiazole Moieties. *Dalton Trans.* **2022**, *51*, 16181–16194. [CrossRef] [PubMed]
42. Von der Stück, R.; Krause, M.; Brünink, D.; Buss, S.; Doltsinis, N.L.; Strassert, C.A.; Klein, A. Luminescent Pd(II) Complexes of Tridentate ⁻CˆNˆN Aryl-pyridine-(benzo)thiazole Ligands. *Z. Allgem. Anorg. Chem.* **2022**, *648*, e202100278. [CrossRef]
43. Mroz, R.; Vezzu, D.A.K.; Wallace, B.; Ravindranathan, D.; Carroll, J.; Pike, R.D.; Huo, S. A Comparative Study on Phosphorescent Cycloplatinated Complexes Based on Tridentate CˆNˆN-Coordinating Ligands and Phenylethynyl or Phenyl Ligand. *Chin. J. Org. Chem.* **2018**, *38*, 171–182. [CrossRef]
44. Zhang, W.; Wang, J.; Xu, Y.; Li, W.; Shen, W. Fine tuning phosphorescent properties of platinum complexes via different N-heterocyclic-based CˆNˆN ligands. *J. Organomet. Chem.* **2017**, *836–837*, 26–33. [CrossRef]
45. Feuerstein, W.; Breher, F. Synthetic access to a phosphorescent non-palindromic pincer complex of palladium by a double oxidative addition—Comproportionation sequence. *Chem. Commun.* **2020**, *56*, 12589. [CrossRef]
46. Rappoport, Z. (Ed.) *CRC Handbook of Tables for Organic Compound Identification*, 3rd ed.; CRC Press/Taylor and Francis: Boca Raton, FL, USA, 1984; ISBN 0-8493-0303-6.
47. Klein, A.; Kaiser, A.; Sarkar, B.; Wanner, M.; Fiedler, J. The Electrochemical Behaviour of Organonickel Complexes: Mono-, Di- and Trivalent Nickel. *Eur. J. Inorg. Chem.* **2007**, *2007*, 965–976. [CrossRef]
48. Huang, H.; Alvarez-Hernandez, J.L.; Hazari, N.; Mercado, B.Q.; Uehling, M.R. Effect of 6,6′-Substituents on Bipyridine-Ligated Ni Catalysts for Cross-Electrophile Coupling. *ACS Catal.* **2024**, *14*, 6897–6914. [CrossRef] [PubMed]
49. Koopmans, T. Über die Zuordnung von Wellenfunktionen und Eigenwerten zu den Einzelnen Elektronen Eines Atoms. *Physica* **1934**, *1*, 104–113. [CrossRef]
50. Janak, J.F. Proof that ∂E/∂ni = ε in density-functional theory. *Phys. Rev. B* **1978**, *18*, 7165–7168. [CrossRef]
51. Tsuneda, T.; Song, J.-W.; Suzuki, S.; Hirao, K. On Koopmans' theorem in density functional theory. *J. Chem. Phys.* **2010**, *133*, 174101. [CrossRef] [PubMed]
52. Thapa, S.; Kafle, A.; Gurung, S.K.; Montoya, A.; Riedel, P.; Giri, R. Ligand-Free Copper-Catalyzed Negishi Coupling of Alkyl-, Aryl-, and Alkynylzinc Reagents with Heteroaryl Iodides. *Angew. Chem. Int. Ed.* **2015**, *54*, 8236–8240. [CrossRef] [PubMed]
53. Dhungana, R.K.; Sapkota, R.R.; Wickham, L.M.; Niroula, D.; Giri, R. Ni-Catalyzed Regioselective 1,2-Dialkylation of Alkenes Enabled by the Formation of Two C(sp^3)-C(sp^3) Bonds. *J. Am. Chem. Soc.* **2020**, *142*, 20930–20936. [CrossRef]
54. Andersen, T.L.; Donslund, A.S.; Neumann, K.T.; Skrydstrup, T. Carbonylative Coupling of Alkyl Zinc Reagents with Benzyl Bromides Catalyzed by a Nickel/NN_2 Pincer Ligand Complex. *Angew. Chem. Int. Ed.* **2018**, *57*, 800–804. [CrossRef] [PubMed]
55. Eckert, P.; Sharif, S.; Organ, M.G. Salt to Taste: The Critical Roles Played by Inorganic Salts in Organozinc Formation and in the Negishi Reaction. *Angew. Chem. Int. Ed.* **2021**, *60*, 12224–12241. [CrossRef] [PubMed]
56. Achonduh, G.T.; Hadei, N.; Valente, C.; Avola, S.; O'Brien, C.J.; Organ, M.G. On the role of additives in alkyl-alkyl Negishi crosscouplings. *Chem. Commun.* **2010**, *46*, 4109–4111. [CrossRef] [PubMed]
57. Plunkett, S.; Basch, C.H.; Santana, S.O.; Watson, M.P. Harnessing Alkylpyridinium Salts as Electrophiles in Deaminative Alkyl−Alkyl Cross-Couplings. *J. Am. Chem. Soc.* **2019**, *141*, 2257–2262. [CrossRef] [PubMed]
58. Chen, L.-M.; Reisman, S.E. Enantioselective C(sp^2)−C(sp^3) Bond Construction by Ni Catalysis. *Acc. Chem. Res.* **2024**, *57*, 751–762. [CrossRef]
59. *APEX4—Software Suite for Crystallographic Programs*; Bruker AXS, Inc.: Madison, WI, USA, 2021.
60. Sheldrick, G.M. SHELXT—Integrated space-group and crystal-structure determination. *Acta Crystallogr. A. Found. Adv.* **2015**, *71*, 3–8. [CrossRef] [PubMed]
61. Sheldrick, G.M. A short history of SHELX. *Acta Crystallogr. A. Found. Adv.* **2008**, *64*, 112–122. [CrossRef] [PubMed]
62. Sheldrick, G.M. Crystal structure refinement with SHELXL. *Acta Crystallogr. C Struct. Chem.* **2015**, *71*, 3–8. [CrossRef]
63. Neese, F.; Wennmohs, F.; Becker, U.; Riplinger, C. The ORCA quantum chemistry program package. *J. Chem. Phys.* **2020**, *152*, 224108. [CrossRef] [PubMed]
64. Neese, F. Software update: The ORCA program system—Version 5.0. *WIREs Comput. Mol. Sci.* **2022**, *12*, e1606. [CrossRef]
65. Weigend, F.; Ahlrichs, R. Balanced basis sets of split valence, triple zeta valence and quadruple zeta valence quality for H to Rn: Design and assessment of accuracy. *Phys. Chem. Chem. Phys.* **2005**, *7*, 3297. [CrossRef]
66. Becke, A.D. Density-functional exchange-energy approximation with correct asymptotic behavior. *Phys. Rev. A* **1988**, *38*, 3098–3100. [CrossRef] [PubMed]

67. Perdew, J.P.; Yue, W. Accurate and simple density functional for the electronic exchange energy: Generalized gradient approximation. *Phys. Rev. B* **1986**, *33*, 8800–8802. [CrossRef] [PubMed]
68. Grimme, S.; Antony, J.; Ehrlich, S.; Krieg, H. A consistent and accurate ab initio parametrization of density functional dispersion correction (DFT-D) for the 94 elements H-Pu. *J. Chem. Phys.* **2010**, *132*, 154104. [CrossRef] [PubMed]
69. Grimme, S.; Ehrlich, S.; Goerigk, L. Effect of the damping function in dispersion corrected density functional theory. *J. Comput. Chem.* **2011**, *32*, 1456–1465. [CrossRef] [PubMed]
70. Barone, V.; Cossi, M. Quantum Calculation of Molecular Energies and Energy Gradients in Solution by a Conductor Solvent Model. *J. Phys. Chem. A* **1998**, *102*, 1995–2001. [CrossRef]
71. Cossi, M.; Rega, N.; Scalmani, G.; Barone, V. Energies, structures, and electronic properties of molecules in solution with the C-PCM solvation model. *J. Comput. Chem.* **2003**, *24*, 669–681. [CrossRef] [PubMed]
72. Tao, J.; Perdew, J.P.; Stavoverov, V.N.; Scuseria, G.E. Climbing the density functional ladder: Nonempirical meta-generalized gradient approximation designed for molecules and solids. *Phys. Rev. Lett.* **2003**, *91*, 146401. [CrossRef] [PubMed]
73. Chemcraft—Graphical Software for Visualization of Quantum Chemistry Computations V1.8. Available online: https://www.chemcraftprog.com (accessed on 28 January 2025).

Disclaimer/Publisher's Note: The statements, opinions and data contained in all publications are solely those of the individual author(s) and contributor(s) and not of MDPI and/or the editor(s). MDPI and/or the editor(s) disclaim responsibility for any injury to people or property resulting from any ideas, methods, instructions or products referred to in the content.